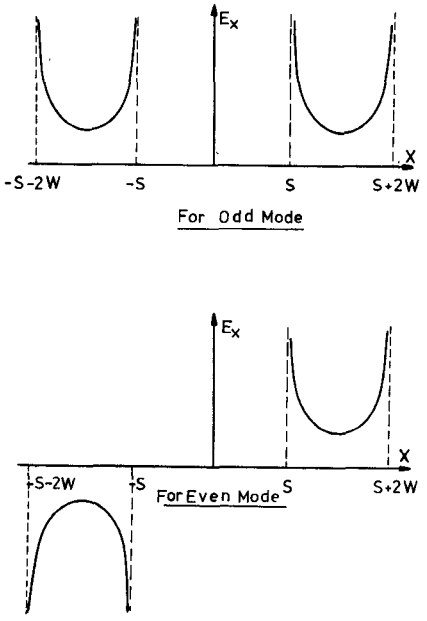

Fig. 3. Distribution of electric field for coupled slots.

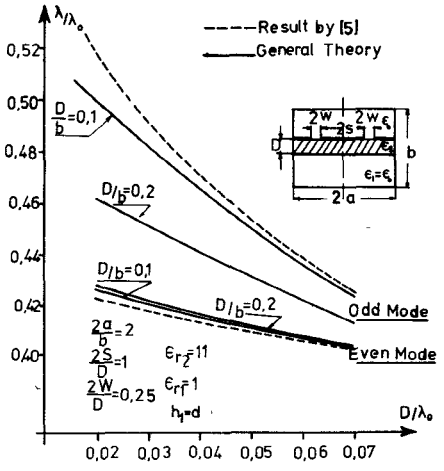

Fig. 4. Even and odd mode dispersion characteristics for coupled slots (even denoting an even E_z, E_y, and H_x).

is consistent with the decreasing effect of the enclosing conductor.

Computing time is about 2 s for each point, and shows the high efficiency of the spectral domain method. There is a clear advantage in the analysis accounting for the enclosing conducting walls, to model the inevitable packaging in practice.

Dispersion characteristics of another type of structure, a shielded coupled slot line, was also investigated. The field distribution within the slots for even and odd modes is shown in Fig. 3, using the dependence $(x^2 - w^2)^{-1/2}$ of [5] and [7]. Fig. 4 shows our results; again a comparison with results of Knorr and Kuchler [5] for open slot lines is given. Computing time for this case is about 6 s per point.

Conclusion

In spite of the increasing interest in suspended substrate transmission line, previous theories have ignored either dispersion, or the presence of the (inevitable) enclosure. The work described here—an extension of the spectral domain approach—allows for efficient computation of slot line, coplanar guide, microstrip, or similar structures (including couplers) with adjacent conductors on the one substrate surface. One computer program deals with an arbitrary number of regions under the coplanar conductors, with simple modifications for different conductors. CPU time on an IBM 360/65 is about 1 s per region for a single slot or strip, at one frequency.

References

[1] H. A. Wheeler, "Transmission-line properties of parallel strips separated by a dielectric sheet," *IEEE Trans. Microwave Theory Tech.*, vol. MTT-13, pp. 172–185, Mar. 1965.
[2] E. Yamashita and R. Mittra, "Variational method for the analysis of microstrip lines," *IEEE Trans. Microwave Theory Tech.*, vol. MTT-16, pp. 251–256, Apr. 1968.
[3] J. Denlinger, "A frequency dependent solution for microstrip transmission lines," *IEEE Trans. Microwave Theory Tech.*, vol. MTT-19, pp. 30–39, Jan. 1971.
[4] T. Itoh and R. Mittra, "A technique for computing dispersion characteristics of shielded microstrip lines," *IEEE Trans. Microwave Theory Tech.*, vol. MTT-22, pp. 896–898, Oct. 1974.
[5] J. B. Knorr and K. D. Kuchler, "Analysis of coupled slots and coplanar strip on dielectric substrate," *IEEE Trans. Microwave Theory Tech.*, vol. MTT-23, pp. 541–547, July 1975.
[6] A. Farrar and A. T. Adams, "Multilayer microstrip transmission lines," *IEEE Trans. Microwave Theory Tech.*, vol. MTT-22, pp. 889–891, Oct. 1974.
[7] T. Itoh and R. Mittra, "Dispersion characteristics of slot lines," *Electron. Lett.*, vol. 7, pp. 364–365, July 1971.

Application of MIC Formulas to a Class of Integrated-Optics Modulator Analyses: A Simple Transformation

EIKICHI YAMASHITA, MEMBER, IEEE,
KAZUHIKO ATSUKI, AND TETSURO MORI

***Abstract*—Modulation electric fields in a class of planar, lumped-parameter circuit or traveling-wave-type electrooptic modulators in integrated optics are analyzed by applying a simple transformation of variables to presently available formulas on microwave integrated circuits (MIC's). Example calculations are shown.**

I. Introduction

It has already been shown that the microwave theory is useful in designing a discrete broad-band electrooptic modulator [1]. Electrooptic modulators in integrated optics are inherently of the planar structure fabricated by microelectronic technology [2]–[6]. While modulators with coplanar electrodes of a narrow gap are expected to have high values of energy efficiency, the nonuniform modulation electric field distribution in the cross section of an optical beam is also apparent.

It is necessary to develop a theory to estimate the electric field distribution in these structures, but such a theory has not been reported. Though there is a structural similarity between such modulators in integrated optics and striplines in microwave integrated circuits (MIC's), the electric field theory of the latter cannot be directly applied to the former since the electrooptic crystal is anisotropic.

This short paper describes a simple transformation of a coordinate and dielectric constants which enables us to apply available formulas and computer programs on MIC's to a class of integrated-optics modulator analyses. Numerical examples based on this method are shown.

Manuscript received February 11, 1976; revised July 6, 1976. This work was supported in part by the Research Project on Laser Communications.
The authors are with the Department of Applied Electronics, University of Electro-Communications, Chofu-shi, Tokyo, Japan.

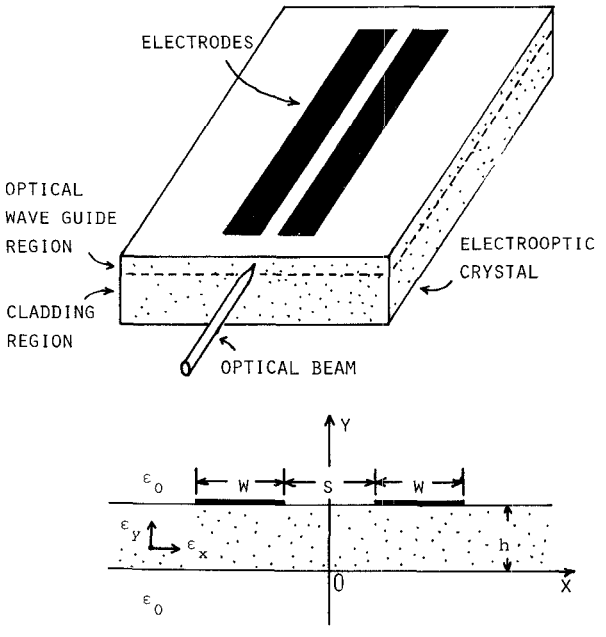

Fig. 1. A typical modulator structure in integrated optics.

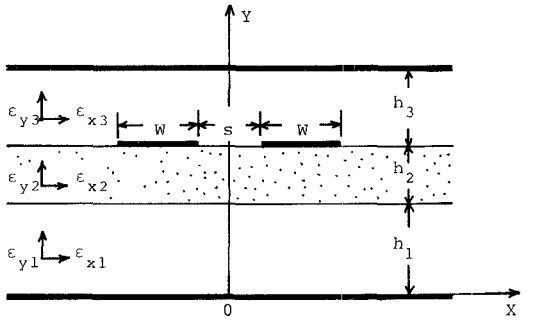

Fig. 2. Multilayer anisotropic structure model for integrated-optics modulators.

II. Modulator Structures

A typical modulator structure which would be used in integrated optics is shown in Fig. 1. Usually, strip electrodes are deposited on an electrooptic crystal such as $LiNbO_3$. An optical waveguide is made on the surface of the crystal by adding a small variation of the index of refraction [2], [6]. The principal axes of the crystal are set in the direction parallel and perpendicular to the crystal surface in many cases.

Basic equations for analyzing the electric field distribution in the crystal are derived from the charge-free condition in the dielectric region. Because the variation of the index of refraction in optical waveguides is small, it can be neglected for the calculation of the modulation electric field. When the electrode is long enough and the principal axes are in the x and y directions, the potential in the crystal is governed approximately by the two-dimensional Laplace's equation

$$\varepsilon_x \frac{\partial^2 \phi}{\partial x^2} + \varepsilon_y \frac{\partial^2 \phi}{\partial y^2} = 0. \tag{1}$$

The electric field distribution and the distributed capacitance are obtained by solving this equation.

III. Transformation from Anisotropic to Equivalent Isotropic Structures

We consider a multilayer structure as shown in Fig. 2 as a model to analyze electrooptic modulators in integrated optics. Any layer in it can be anisotropic or isotropic by imposing a condition, $\varepsilon_x \neq \varepsilon_y$ or $\varepsilon_x = \varepsilon_y$, respectively. The principal axes of each uniaxial crystal are assumed to be in the direction of the two coordinates. The strip electrodes are assumed to be negligibly thin and they are inserted between these layers. Side walls are not assumed in this case for simplicity. However, if the side walls are present, the essential points of discussion will not be changed.

Laplace's equations for these layers are given by

$$\varepsilon_{x1} \frac{\partial^2 \phi}{\partial x^2} + \varepsilon_{y1} \frac{\partial^2 \phi}{\partial y^2} = 0, \qquad 0 \le y \le h_1 \tag{2a}$$

$$\varepsilon_{x2} \frac{\partial^2 \phi}{\partial x^2} + \varepsilon_{y2} \frac{\partial^2 \phi}{\partial y^2} = 0, \qquad h_1 \le y \le h_1 + h_2 \tag{2b}$$

$$\varepsilon_{x3} \frac{\partial^2 \phi}{\partial x^2} + \varepsilon_{y3} \frac{\partial^2 \phi}{\partial y^2} = 0, \qquad h_1 + h_2 \le y \le h_1 + h_2 + h_3. \tag{2c}$$

When the charge distribution functions on the strip electrodes are denoted by $f(x)$, then the boundary conditions are given by

$$\varepsilon_{y1} \left.\frac{\partial \phi}{\partial y}\right|_{y=h_1-0} = \varepsilon_{y2} \left.\frac{\partial \phi}{\partial y}\right|_{y=h_1+0} \tag{3a}$$

$$\varepsilon_{y2} \left.\frac{\partial \phi}{\partial y}\right|_{y=h_1+h_2-0} = \varepsilon_{y3} \left.\frac{\partial \phi}{\partial y}\right|_{y=h_1+h_2+0} - f(x) \tag{3b}$$

$$\left.\frac{\partial \phi}{\partial x}\right|_{y=h_1-0} = \left.\frac{\partial \phi}{\partial x}\right|_{y=h_1+0} \tag{3c}$$

$$\left.\frac{\partial \phi}{\partial x}\right|_{y=h_1+h_2-0} = \left.\frac{\partial \phi}{\partial x}\right|_{y=h_1+h_2+0} \tag{3d}$$

$$\phi|_{y=0} = 0 \tag{3e}$$

$$\phi|_{y=h_1+h_2+h_3} = 0. \tag{3f}$$

Because of the anisotropic nature of this structure, various methods used in the MIC analyses cannot be directly applied to these equations. Therefore, we newly define a transformation of the variable y in Laplace's equations (an affine transformation) and the dielectric constants in the following form:

$$\eta = \sqrt{\frac{\varepsilon_{x1}}{\varepsilon_{y1}}}\, y, \qquad 0 \le y \le h_1 \tag{4a}$$

$$\eta = \sqrt{\frac{\varepsilon_{x1}}{\varepsilon_{y1}}}\, h_1 + \sqrt{\frac{\varepsilon_{x2}}{\varepsilon_{y2}}}\,(y - h_1), \qquad h_1 \le y \le h_1 + h_2 \tag{4b}$$

$$\eta = \sqrt{\frac{\varepsilon_{x1}}{\varepsilon_{y1}}}\, h_1 + \sqrt{\frac{\varepsilon_{x2}}{\varepsilon_{y2}}}\, h_2 + \sqrt{\frac{\varepsilon_{x3}}{\varepsilon_{y3}}}\,(y - h_1 - h_2), \qquad h_1 + h_2 \le y \le h_1 + h_2 + h_3 \tag{4c}$$

$$\varepsilon_1 = \sqrt{\varepsilon_{x1}\varepsilon_{y1}} \tag{5a}$$

$$\varepsilon_2 = \sqrt{\varepsilon_{x2}\varepsilon_{y2}} \tag{5b}$$

$$\varepsilon_3 = \sqrt{\varepsilon_{x3}\varepsilon_{y3}}. \tag{5c}$$

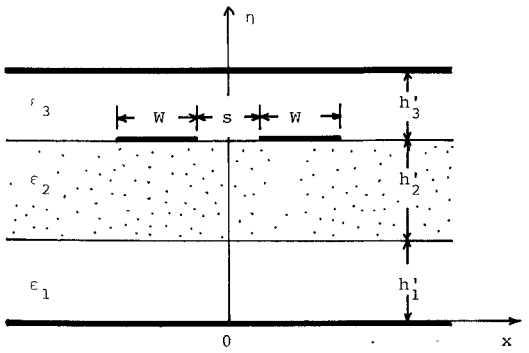

Fig. 3. Equivalent multilayer isotropic structure transformed from the anisotropic structure in Fig. 2 by the relations in (5) and (8).

As a result of these transformations, Laplace's equations in (2) and the boundary conditions in (3) are modified as follows:

$$\frac{\partial^2\phi}{\partial x^2} + \frac{\partial^2\phi}{\partial \eta^2} = 0, \qquad 0 \le \eta \le h_1' + h_2' + h_3' \tag{6}$$

$$\varepsilon_1 \left.\frac{\partial\phi}{\partial\eta}\right|_{\eta=h_1'-0} = \varepsilon_2 \left.\frac{\partial\phi}{\partial\eta}\right|_{\eta=h_1'+0} \tag{7a}$$

$$\varepsilon_2 \left.\frac{\partial\phi}{\partial\eta}\right|_{\eta=h_1'+h_2'-0} = \varepsilon_3 \left.\frac{\partial\phi}{\partial\eta}\right|_{\eta=h_1'+h_2'+0} - f(x) \tag{7b}$$

$$\left.\frac{\partial\phi}{\partial\eta}\right|_{\eta=h_1'-0} = \left.\frac{\partial\phi}{\partial\eta}\right|_{\eta=h_1'+0} \tag{7c}$$

$$\left.\frac{\partial\phi}{\partial\eta}\right|_{\eta=h_1'+h_2'-0} = \left.\frac{\partial\phi}{\partial\eta}\right|_{\eta=h_1'+h_2'+0} \tag{7d}$$

$$\phi|_{\eta=0} = 0 \tag{7e}$$

$$\phi|_{\eta=h_1'+h_2'+h_3'} = 0 \tag{7f}$$

where

$$h_1' = \sqrt{\frac{\varepsilon_{x1}}{\varepsilon_{y1}}}\, h_1 \tag{8a}$$

$$h_2' = \sqrt{\frac{\varepsilon_{x2}}{\varepsilon_{y2}}}\, h_2 \tag{8b}$$

$$h_3' = \sqrt{\frac{\varepsilon_{x3}}{\varepsilon_{y3}}}\, h_3. \tag{8c}$$

The isotropic multilayer structure, as shown in Fig. 3, corresponds to (6) and the boundary conditions (7).

The electric field distribution in this type of structure has been well analyzed by the variational method [7], the integral equation method [8], the generalized Wiener–Hopf method [9], the finite difference method [10], the conformal mapping [11], etc. Therefore, many formulas and computation programs based on these methods are readily applicable to the present case.

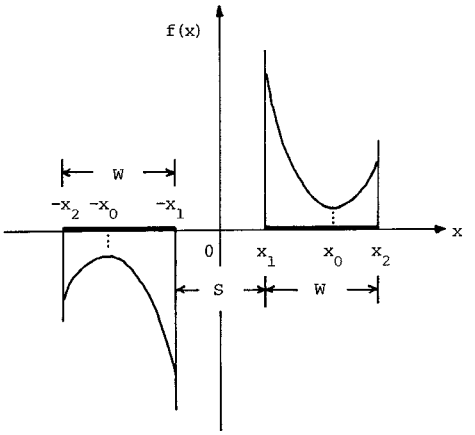

Fig. 4. Possible charge distribution function on electrodes.

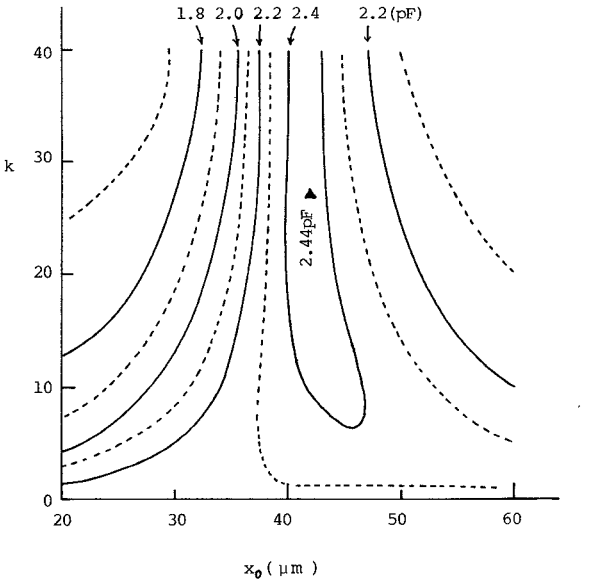

Fig. 5. Capacitance per unit length C plotted as a function of k and x_0.

IV. Distributed Capacitance of Three-Layer Structure

We show a formula for the distributed capacitance of the three-layer structure in Fig. 2, for example. Since a stationary value expression of the capacitance per unit length in the Fourier transform domain has been given in [7], we apply the transformations in (5) and (8) to that expression and readily obtain

$$\frac{1}{C} = \frac{1}{2\pi Q^2} \int_{-\infty}^{+\infty} |\tilde{f}(\beta)|^2 \tilde{g}(\beta)\, d\beta \tag{9}$$

where

$$\tilde{f}(\beta) = \int_{-\infty}^{+\infty} f(x) e^{j\beta x}\, d\beta \tag{10}$$

$$Q = \int f(x)\, dx \quad \text{(the total charge on one electrode)} \tag{11}$$

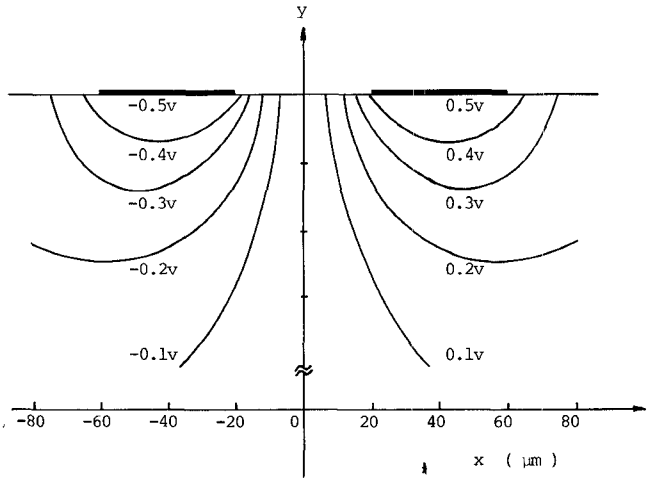

Fig. 6. Potential distribution near electrodes.

and

$$\tilde{g}(\beta) = \frac{\sqrt{\varepsilon_{x1}\varepsilon_{y1}}\coth\left(\sqrt{\frac{\varepsilon_{x1}}{\varepsilon_{y1}}}|\beta|h_1\right) + \sqrt{\varepsilon_{x2}\varepsilon_{y2}}\coth\left(\sqrt{\frac{\varepsilon_{x2}}{\varepsilon_{y2}}}|\beta|h_2\right)}{|\beta|\left\{\sqrt{\varepsilon_{x1}\varepsilon_{y1}}\coth\left(\sqrt{\frac{\varepsilon_{x1}}{\varepsilon_{y1}}}|\beta|h_1\right)\left[\sqrt{\varepsilon_{x3}\varepsilon_{y3}}\coth\left(\sqrt{\frac{\varepsilon_{x3}}{\varepsilon_{y3}}}|\beta|h_3\right) + \sqrt{\varepsilon_{x2}\varepsilon_{y2}}\coth\left(\sqrt{\frac{\varepsilon_{x2}}{\varepsilon_{y2}}}|\beta|h_2\right)\right] + \sqrt{\varepsilon_{x2}\varepsilon_{y2}}\left[\sqrt{\varepsilon_{x2}\varepsilon_{y2}} + \sqrt{\varepsilon_{x3}\varepsilon_{y3}}\coth\left(\sqrt{\frac{\varepsilon_{x2}}{\varepsilon_{y2}}}|\beta|h_2\right)\coth\left(\sqrt{\frac{\varepsilon_{x3}}{\varepsilon_{y3}}}|\beta|h_3\right)\right]\right\}}. \quad (12)$$

V. Coplanar Electrode Structure

Let us investigate numerical values of modulation fields between the two electrodes of the structure in Fig. 1. This structure is a special case of the structure in Fig. 2. Therefore, the distributed capacitance is derived from the formula (9) and $\tilde{g}(\beta)$ given by

$$\tilde{g}(\beta) = \frac{\varepsilon_0 + \sqrt{\varepsilon_x\varepsilon_y}\coth\left(\sqrt{\frac{\varepsilon_x}{\varepsilon_y}}|\beta|h\right)}{|\beta|\left\{\varepsilon_0^2 + \varepsilon_x\varepsilon_y + 2\varepsilon_0\sqrt{\varepsilon_x\varepsilon_y}\coth\left(\sqrt{\frac{\varepsilon_x}{\varepsilon_y}}\beta|h|\right)\right\}}. \quad (13)$$

The trial function $f(x)$ is selected so as to maximize the capacitance C in (9). Since the charge density near conductor edges should be very high, as shown in Fig. 4, $f(x)$ is approximated by

$$f(x) = 1 + k\left|\frac{x - x_0}{x_2 - x_1}\right|^3, \qquad x_1 \le x \le x_2$$
$$= -1 - k\left|\frac{x + x_0}{x_2 - x_1}\right|^3, \qquad -x_2 \le x \le -x_1$$
$$= 0, \qquad \text{otherwise} \quad (14)$$

where k and x_0 are chosen so as to maximize C. Then, Q and $\tilde{f}(\beta)$ are given by

$$Q = (x_2 - x_1) + \frac{k}{4(x_2 - x_1)^3}\{(x_0 - x_1)^4 + (x_2 - x_0)^4\} \quad (15)$$

$$\tilde{f}(\beta) = j\frac{4}{\beta}\sin\left\{\frac{\beta}{2}(x_2 - x_1)\right\}\sin\left\{\frac{\beta}{2}(x_2 + x_1)\right\} + j\frac{k}{(x_2 - x_1)} \cdot \left(\frac{24}{\beta^4}\sin(\beta x_0) + \left\{\frac{6}{\beta^2}(x_0 - x_1)^2 - \frac{12}{\beta^4}\right\}\sin(\beta x_1) + \left\{\frac{2}{\beta}(x_0 - x_1)^3 - \frac{12}{\beta^3}(x_0 - x_1)\right\}\cos(\beta x_1) + \left\{\frac{6}{\beta^2}(x_2 - x_0)^2 - \frac{12}{\beta^4}\right\}\sin(\beta x_2) - \left\{\frac{2}{\beta}(x_2 - x_0)^3 - \frac{12}{\beta^3}(x_2 - x_0)\right\}\cos(\beta x_2)\right). \quad (16)$$

Fig. 5 shows computed results of C as a function of k and x_0 where structural constants are given as $\varepsilon_x^* = 28$, $\varepsilon_y^* = 43$, $h = 2$ mm, $W = s = 40$ μm, $x_1 = 20$ μm, $x_2 = 60$ μm. Consequently, the maximum value of C is 2.44 pF/cm for $k = 27$ and $x_0 = 42$ μm.

The potential distribution $\phi(x,y)$ is given by the inverse Fourier transform of $\tilde{\phi}(\beta,y)$ as

$$\phi(x,y) = \frac{1}{2\pi}\int_{-\infty}^{+\infty}\tilde{\phi}(\beta,y)e^{-j\beta x}\,d\beta \quad (17)$$

where

$$\tilde{\phi}(\beta,y) = \frac{\tilde{f}(\beta)}{|\beta|}\frac{\varepsilon_0\sinh\left(\sqrt{\frac{\varepsilon_x}{\varepsilon_y}}|\beta|y\right) + \sqrt{\varepsilon_x\varepsilon_y}\cosh\left(\sqrt{\frac{\varepsilon_x}{\varepsilon_y}}|\beta|y\right)}{(\varepsilon_0^2 + \varepsilon_x\varepsilon_y)\sinh\left(\sqrt{\frac{\varepsilon_x}{\varepsilon_y}}|\beta|h\right) + 2\varepsilon_0\sqrt{\varepsilon_x\varepsilon_y}\cosh\left(\sqrt{\frac{\varepsilon_x}{\varepsilon_y}}|\beta|h\right)}. \quad (18)$$

Fig. 6 shows the computed results of the potential distribution near the electrodes. It is noted that the potential values are less accurate than the capacitance values because of the variational method. Fig. 7 shows the electric field distribution based on Fig. 6. The nonuniformity of electric fields seen in Fig. 7 also suggests irregular modulation effects in the cross section of an optical beam passing between the electrodes.

When such an electrooptical modulator of length L is incorporated in a circuit as a lumped element, the bandwidth of this modulator is given by $(\pi CRL)^{-1}$ where R is the parallel

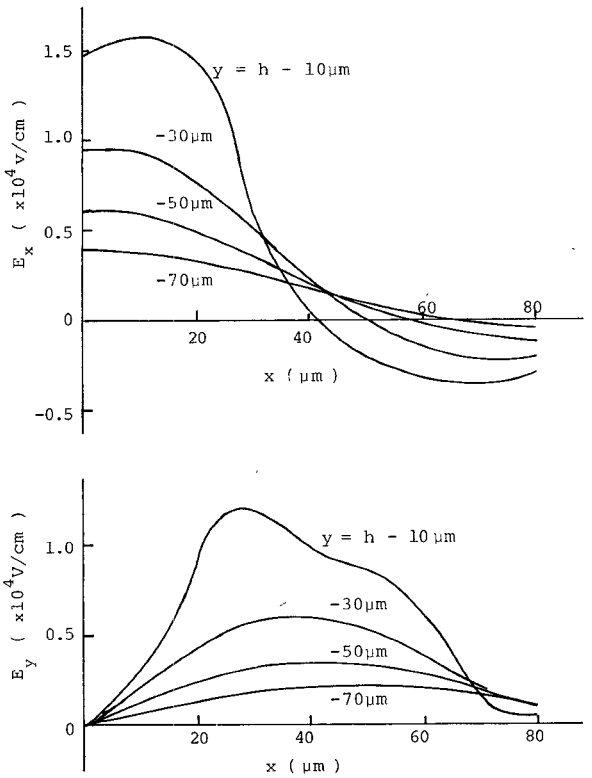

Fig. 7. Electric field distribution near electrodes.

resistance connected between the electrodes [5]. Since the dimensions of the electrodes can be made extremely small by microelectronics techniques, the modulation bandwidth Δf can be large and the required modulation power P can be small. Therefore, effective modulators with a low value of $P/\Delta f$ can be expected for a thin optical beam.

When the uniform electrooptic effects in the cross section of a passing optical beam are required, however, the electrode spacing has to be increased. As a result, the increase of $P/\Delta f$ is inevitable.

VI. Traveling-Wave Structures

When the modulation frequency is high so that the wavelength becomes comparable to the electrode length, the modulator can be treated as a transmission line. The two important quantities of traveling-wave modulators are the modulation wave velocity v and the characteristic impedance Z. These are, within the TEM wave approximation, obtained from the preceding capacitance and the formulas [7]

$$v = \sqrt{\frac{C_0}{C}}\, v_0 \tag{19}$$

$$Z = \frac{1}{v_0\sqrt{CC_0}} \tag{20}$$

where v_0 is the velocity of light in vacuum, C is the capacitance per unit length of the transmission line, and the C_0 is the capacitance per unit length for the same transmission line conductors in vacuum. The velocity of modulation waves is designed to match that of light in the crystal for the traveling-wave modulation.

If the two matching conditions on the velocity and impedance [1] are satisfied by selecting the dimensions of the modulator, the coplanar electrode modulator with a very narrow gap is expected to be of high efficiency and broad bandwidth.

References

[1] E. Yamashita, K. Atsuki, and T. Akamatsu, "Application of microstrip analysis to the design of a broad-band electrooptical modulator," *IEEE Trans. Microwave Theory Tech.*, vol. MTT-22, pp. 462–464, Apr. 1974.
[2] I. P. Kaminow, J. R. Carrutheres, E. H. Turner, and L. W. Statz, "Thin-film $LiNbO_3$ electro-optic modulator," *Appl. Phys. Lett.*, vol. 22, pp. 540–542, May 1973.
[3] E. Yamashita and K. Atsuki, "Distributed capacitance of a thin-film electrooptic light modulator," *IEEE Trans. Microwave Theory Tech.*, vol. MTT-23, pp. 177–178, Jan. 1975.
[4] W. E. Martin, "A new waveguide switch/modulator for integrated optics," *Appl. Phys. Lett.*, vol. 26, pp. 562–564, May 1975.
[5] M. K. Barnoski, *Introduction to Integrated Optics*. Plenum Press, 1974, ch. 13.
[6] T. Tamir, *Integrated Optics*. Springer-Verlag, 1975, ch. 4.
[7] E. Yamashita, "Variational method for the analysis of microstrip-like transmission lines," *IEEE Trans. Microwave Theory Tech.*, vol. MTT-16, pp. 529–535, Aug. 1968.
[8] E. Yamashita and K. Atsuki, "Analysis of thick-strip transmission lines," *IEEE Trans. Microwave Theory Tech.*, vol. MTT-19, pp. 120–122, Jan. 1971
[9] R. Mittra and T. Itoh, "Charge and potential distributions in shielded strip lines," *IEEE Trans. Microwave Theory Tech.*, vol. MTT-18, pp. 149–156, Mar. 1970.
[10] H. E. Stinehelfer, Sr., "An accurate calculation of uniform microstrip transmission lines," *IEEE Trans. Microwave Theory Tech.*, vol. MTT-16, pp. 439–444, July 1968.
[11] H. A. Wheeler, "Transmission-line properties of parallel strips separated by a dielectric sheet," *IEEE Trans. Microwave Theory Tech.*, vol. MTT-13, pp. 172–185, Mar. 1965.
[12] W. S. C. Chang, "Integrated optics at 10.6-μm wavelength," *IEEE Trans. Microwave Theory Tech.*, vol. MTT-23, pp. 31–44, Jan. 1975.

Central Metal Post in Stripline Circulators

ALI M. HUSSEIN, STUDENT MEMBER, IEEE,
MAGDY M. IBRAHIM, MEMBER, IEEE, AND
SAAD E. YOUSSEF

***Abstract*—A central metal post of a suitable radius increases the bandwidth of a 3-port stripline circulator considerably. It helps to realize a compact circulator and gives more flexibility in the design.**

Introduction

The insertion of a central metal post was considered in the design of broad-band 3-port waveguide circulators [1]–[4]. In the case of stripline circulators, the efforts were mainly concentrated to obtain broader bandwidth using external matching elements [5]–[9].

We prove here that the insertion of a central metal post, in the case of 3-port stripline circulators, can increase up to three times the bandwidth of the simple junction. The radius of the ferrite disk can be reduced. Generally, a central metal post gives more flexibility in the design.

Field Analysis and Computational Results

Consider a metal post of radius a placed at the center of a ferrite disk of radius R. The z component of the electric field

Manuscript received June 23, 1975; revised May 10, 1976.
A. M. Hussein was with the Department of Electrical Engineering, Ain-Shams University, Cairo, Egypt. He is now with the Department of Electrical Engineering, University of Toronto, Toronto, Ont., Canada.
M. M. Ibrahim and S. E. Youssef are with the Department of Electrical Engineering, Ain-Shams University, Cairo, Egypt.